A&A 383, 919–932 (2002)
DOI: 10.1051/0004-6361:20011810

Astronomy & Astrophysics

Structure and evolution of FK Comae corona

P. Gondoin, C. Erd, and D. Lumb

Space Science Department, European Space Agency – Postbus 299, 2200 AG Noordwijk, The Netherlands

Received 16 October 2001 / Accepted 17 December 2001

Abstract. FK Comae (HD 117555) is a rapidly rotating single G giant whose distinctive characteristics include a quasisinusoidal optical light curve and high X-ray luminosity. FK Comae was observed twice at two weeks interval in January 2001 by the *XMM-Newton* space observatory. Analysis results suggest a scenario where the corona of FK Comae is dominated by large magnetic structures similar in size to interconnecting loops between solar active regions but significantly hotter. The interaction of these structures themselves could explain the permanent flaring activity on large scales that is responsible for heating FK Comae plasma to high temperatures. During our observations, these flares were not randomly distributed on the star surface but were partly grouped within a large compact region of about 30 degree extent in longitude reminiscent of a large photospheric spot. We argue that the $\alpha - \Omega$ dynamo driven activity on FK Comae will disappear in the future with the effect of suppressing large scale magnetic structures in its corona.

Key words. stars: individual: FK Comae – stars: activity – stars: coronae – stars: evolution – stars: late-type – X-ray: stars

1. Introduction

FK Comae (HD 117555) is the prototype of a small group of single G giants defined by Bopp & Rucinski (1981) as the FK Comae-type stars. FK Comae has been observed in all accessible bands (Bopp & Stencel 1981) from X-rays (Walter 1981) to the radio domain (Hughes & McLean 1987). Its spectral peculiarities include a strong, broad and variable Hα emission (Walter & Basri 1982; Oliveira & Foing 1999), strong UV chromospheric emission lines similar to those seen in the RS CVn binaries (Bopp & Stencel 1981), a quasisinusoidal optical light curve, suggestive of starspots (Holtzman & Nation 1984; Jetsu et al. 1993) and an X-ray luminosity (Walter 1981; Welty & Ramsey 1994) exceptionally high for a red giant. We report on analysis results of X−ray spectra of FK Comae registered during two observations performed in January 2001 by the *XMM-Newton* observatory. This work aims to improve our understanding of the magnetic activity on FK Comae by investigating the origin of its high X-ray luminosity and the structure of its X-ray corona.

Section 2 provides the stellar parameters of FK Comae and compares its possible evolution status with those of nearby single field giants in light of Hipparcos parallaxes (ESA 1997). Section 3 describes the X-ray observations of FK Comae and the data reduction procedures. Section 4 presents the integrated flux measurements and their temporal behaviour during the observations. Sections 5 and 6 describe the spectral analysis of the EPIC and RGS datasets. A physical interpretation of the analysis results is proposed in Sect. 7. In this section, the structure of FK Comae corona and its possible evolution is discussed within the frame of stellar activity evolution across the Hertzsprung gap.

Send offprint requests to: P. Gondoin,
e-mail: pgondoin@astro.estec.esa.nl

2. FK Comae stellar parameters

The must striking peculiarity of FK Comae is its rapid rotation in regard to its spectral type. One hypothesis to explain the rapid rotation and activity of FK Comae is the existence of a tiny but yet unseen companion. This companion would dump mass onto the visible component thus producing a significant angular momentum transfer (Walter & Basri 1982). However, no radial velocity variation characteristic of orbital motion has been detected. The data of McCarthy & Ramsey (1984) and Huenemoeder et al. (1993) have made this small companion hypothesis extremely untenable. Hence, the origin of FK Comae is still a matter of debate. One possible scenario is that the star originates from an early type, rapidly rotating, single star as it evolves in the giant domain (Simon & Drake 1989).

Hipparcos measurements of FK Comae parallax give a distance of 234 pc in agreement with the results by Eggen & Iben (1989) who associated FK Comae with a moving group at a distance of 238 pc. Strassmeier et al. (1997) reported $V = 8.04$ as the brightest V magnitude

Table 1. Top: V magnitudes, parallaxes, extinctions and absolute magnitudes of FK Comae. The brightest V magnitude of the least-spotted photosphere is quoted. Middle: spectral type, color indices and effective temperature. The temperature of the quiescent photosphere outside starspots is given as derived from Doppler imaging techniques. Bottom: estimated stellar parameters of FK Comae.

V	par (mas)	A_V	M_V
8.04	4.27 ± 1.00	0.03	0.69–1.65
Sp. Type	$B-V$	$V-I$	$T_{\rm eff}$ (K)
G5 III	0.870	0.93	5080
L ($L_\odot$)	R ($R_\odot$)	$v_{\rm eq}$ (km s^{-1})	M ($M_\odot$)
21–54	5.9–9.9	124–209	2.0–2.7

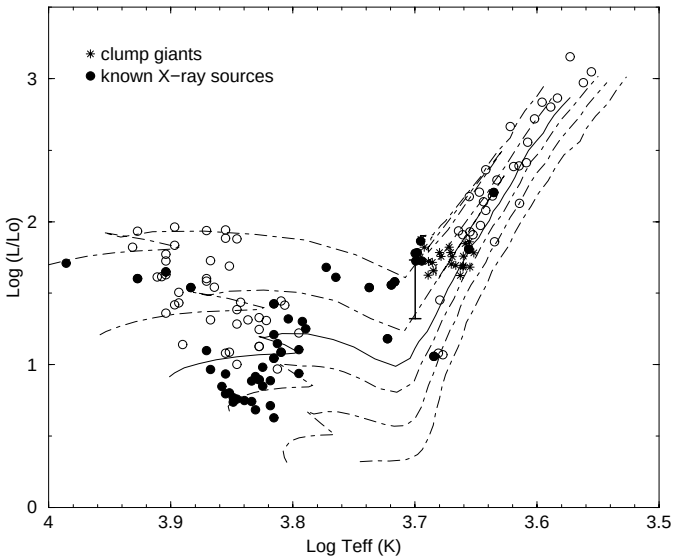

Fig. 1. H-R diagram of single giants (Gondoin 1999) compared with evolutionary tracks (Schaller et al. 1992) of 1 $M_\odot$ (lower dashed line), 1.25 $M_\odot$, 1.5 $M_\odot$, 1.7 $M_\odot$ (solid line), 2 $M_\odot$ and 2.5 $M_\odot$. Black circles mark giants known as X-ray sources. The H-R diagram location of FK Comae is indicated by an error bar.

of FK Comae which is so far the best approximation to the magnitude of the unspotted star. The visual extinction on the line of sight to FK Comae is small since the star is located closed to the North Galactic Pole (NGP). Assuming a NGP extinction $A_{\rm V} = 0.03$ (Burstein & Heiles 1982), we calculated the absolute magnitude of FK Comae from its unspotted V magnitude and Hipparcos parallax. We then derived the star's luminosity (see Table 1) using the bolometric correction vs effective temperature data of Flower (1996). Korhonen et al. (1999) found that the best fit to the average spectrum of FK Comae can be obtained with a microturbulence velocity $v_{\rm micro} = 1.4$ km s^{-1} and $T_{\rm eff} = 5080$ K. This effective temperature of the unspotted photosphere corresponds to the spectral type G5 III and was used to determine the H-R diagram position of the star.

Figure 1 compares the H-R diagram positions of FK Comae and single nearby giants (Gondoin 1999) with evolutionary tracks of stellar models with near solar metallicity (Schaller et al. 1992). FK Comae occupies a particular region near the bottom of the red giant branch (RGB) close to the evolutionary tracks of a 2.0−2.5 $M_\odot$ star. This mass estimate suggests that FK Comae could have rapidly evolved from an early A-type main sequence star. An alternative hypothesis to explain the rapid star rotation is that FK Comae results from merging of a close binary system (Bopp & Stencel 1981) such as a W Ursae Majoris system (Collier Cameron 1982). The high space velocity of FK Comae ($< S > = 82$ km s^{-1}) and its large distance above the galactic plane infer an age ≈5–10 Gyr and give support to this interpretation which predicts $M_V = 1 \pm 1$. Trimble & Kundu (1997) found $M_V = 1.4 \pm 0.5$ for FK Comae in agreement with our $M_V = 1.2 \pm 0.5$ derivation, thus making the binary merger paradigm a possible scenario.

3. Observations and data reduction

FK Comae was observed twice by the *XMM-Newton* space observatory (Jansen et al. 2001), respectively in revolution 199 on 2001 January 8 and in revolution 205 on 2001 January 21 (see Table 2). The satellite observatory uses three grazing incidence telescopes which provide an effective area higher than 4000 cm^2 at 2 keV and 1600 cm^2 at 8 keV (Gondoin et al. 2000). Three CCD EPIC cameras (Strüder et al. 2001; Turner et al. 2001) at the prime focus of the telescopes provide imaging in a 30 arcmin field of view and broadband spectroscopy with a resolving power of between 10 and 60 in the energy band 0.3 to 10 keV. Two identical RGS reflection grating spectrometers behind two of the three X-ray telescopes allow higher resolution ($E/\Delta E$ = 100 to 500) measurements in the soft X-ray range (6 to 38 Å or 0.3 to 2.1 keV) with a maximum effective area of about 140 cm^2 at 15 Å (den Herder et al. 2001). FK Comae observations were conducted with the EPIC cameras operating in full frame mode (Ehle et al. 2001). RGS spectra were recorded simultaneously. "Medium" thickness aluminum filters were used in front of all EPIC cameras to reject visible light. Processing of the raw event dataset was performed using the "emproc", "epproc" and "rgsproc" pipeline tasks of the *XMM-Newton* Science Analysis System (SAS version 5.0.1). Due to the presence of neighbouring sources in the EPIC field of view (HD 117567 and BD+24 2593B at respectively 31″ and 41″ east of the target), FK Comae spectra were built from photons detected within a window of 54″ diameter around the target boresight in the MOS cameras. A smaller 46″ diameter extraction window was used for the p−n data imposed by the proximity of the p−n CCD edges. The background was estimated on the same CCD chips as the source, within windows of the same sizes which were offset from the source position

Table 2. FK Comae observation log during *XMM-Newton* revolution 199 and 205.

Rev.	Experiment	Filter	Mode	Start Exp. (UT)	Exp. Duration
199	MOS1	Medium	Prime Full	01-08@23:40:01	30 024 s
	MOS2	Medium	Prime Full	01-08@23:40:01	30 024 s
	p−n	Medium	Prime Full	01-09@00:21:24	27 918 s
	RGS1		Spec + Q	01-08@23:31:35	30 956 s
	RGS2		Spec + Q	01-08@23:31:35	30 956 s
205	MOS1	Medium	Prime Full	01-21@16:52:57	38 674 s
	MOS2	Medium	Prime Full	01-21@16:52:57	38 674 s
	p−n	Medium	Prime Full	01-21@17:34:20	36 568 s
	RGS1		Spec + Q	01-21@16:44:31	41 456 s
	RGS2		Spec + Q	01-21@16:44:31	41 456 s

Table 3. X-ray luminosities (corrected for interstellar absorption) of FK Comae in the 0.3−2 keV and 2−10 keV energy bands during the different periods. The percentage contribution in luminosity of hot plasmas ($kT > 3$ keV) is indicated between bracketts.

Obs.	$L_{0.3-2\ \mathrm{keV}}$ (10^{30} erg s^{-1})	$L_{2-10\ \mathrm{keV}}$ (10^{30} erg s^{-1})	hr
Rev. 199 (rising cr)	28.1 (85%)	32.5 (99%)	0.07
Rev. 199 (high cr)	45.8 (92%)	55.1 (100%)	0.09
Rev. 205 (low cr)	18.3 (73%)	12.0 (98%)	–0.21
Rev. 205 (flare)	23.2 (73%)	17.8 (99%)	–0.13

in an empty field region. The Pulse-Invariant (PI) spectra were rebinned such that each resulting MOS channel had at least 20 counts per bin and each p−n channel had at least 50 counts per bin. χ^2 minimization was used for spectral fitting. All fits were performed using the XSPEC package (Arnaud & Dorman 2001). We used the EPIC response matrices provided by the PI institutes[1]. The RGS response matrices were generated by the SAS task "rgsrmfgen". EPIC p−n, MOS 1 and MOS 2 spectra were fitted together in the 0.3 to 10 keV energy range. The RGS spectra were analysed separately due to their higher spectral resolution in the 0.3−2.1 keV energy range.

[1] (See *XMM-Newton* Calibration Page at `http://xmm.vilspa.esa.es/calibration`).

4. Integrated flux and temporal behaviour

Figure 2 top shows the light curves of FK Comae obtained during revolution 199 and 205 with the p−n camera. The X-ray flux was strongly variable during both revolutions. Count rates fluctuated by a factor of 2.6 during revolution 199 and by a factor of 2 during revolution 205. The two light curves are different. During revolution 199, the flux increased steadily within the first 15 ksec of the observation up to a high count rate which remained stable for the rest of the exposure at a level of about 2.5 cts s^{-1} (p−n) and 1.3 cts s^{-1} (MOS) in the 0.5 to 2 keV band. On the contrary, during revolution 205, the count rate rapidly increased and decreased during the first 15 ksec of the observation and then remained stable at a relatively low level of about 1.0 cts s^{-1} (p−n) and 0.5 cts s^{-1} (MOS) in the 0.5 to 2 keV band. Hence, we conducted the spectral analysis of each observation separately for two flux levels. The spectral analysis of revolution 199 data was performed in two time intervals when count rates were respectively lower and higher than 2.2 cts s^{-1} in the 500 eV to 2 keV band of the p−n cameras. These intervals correspond to the slowly increasing flux period during the first 10 ksec of the observation and to the steady high level flux period observed at the end. The spectral analysis of revolution 205 data was conducted in two time intervals when count rates were respectively lower and higher than 1.2 cts s^{-1} in the 500 eV to 2 keV band of the p−n cameras. These intervals correspond to the short transient flux increase of about 7 ksec at the beginning of the exposure and to the steady low flux level observed during the remaining part of the observation.

Spectral fitting of EPIC data (see Sect. 5) during these four periods yields flux measurements in the 0.3−2 keV and 2−10 keV bands. These measurements were converted into X-ray luminosities $L_{0.3-2\ \mathrm{keV}}$ and $L_{2-10\ \mathrm{keV}}$ using Hipparcos parallax. Results are given in Table 3 including hardness ratios hr of the X-ray emission defined as $hr = (L_{2-10\ \mathrm{keV}} - L_{0.3-2\ \mathrm{keV}})/(L_{2-10\ \mathrm{keV}} + L_{0.3-2\ \mathrm{keV}})$.

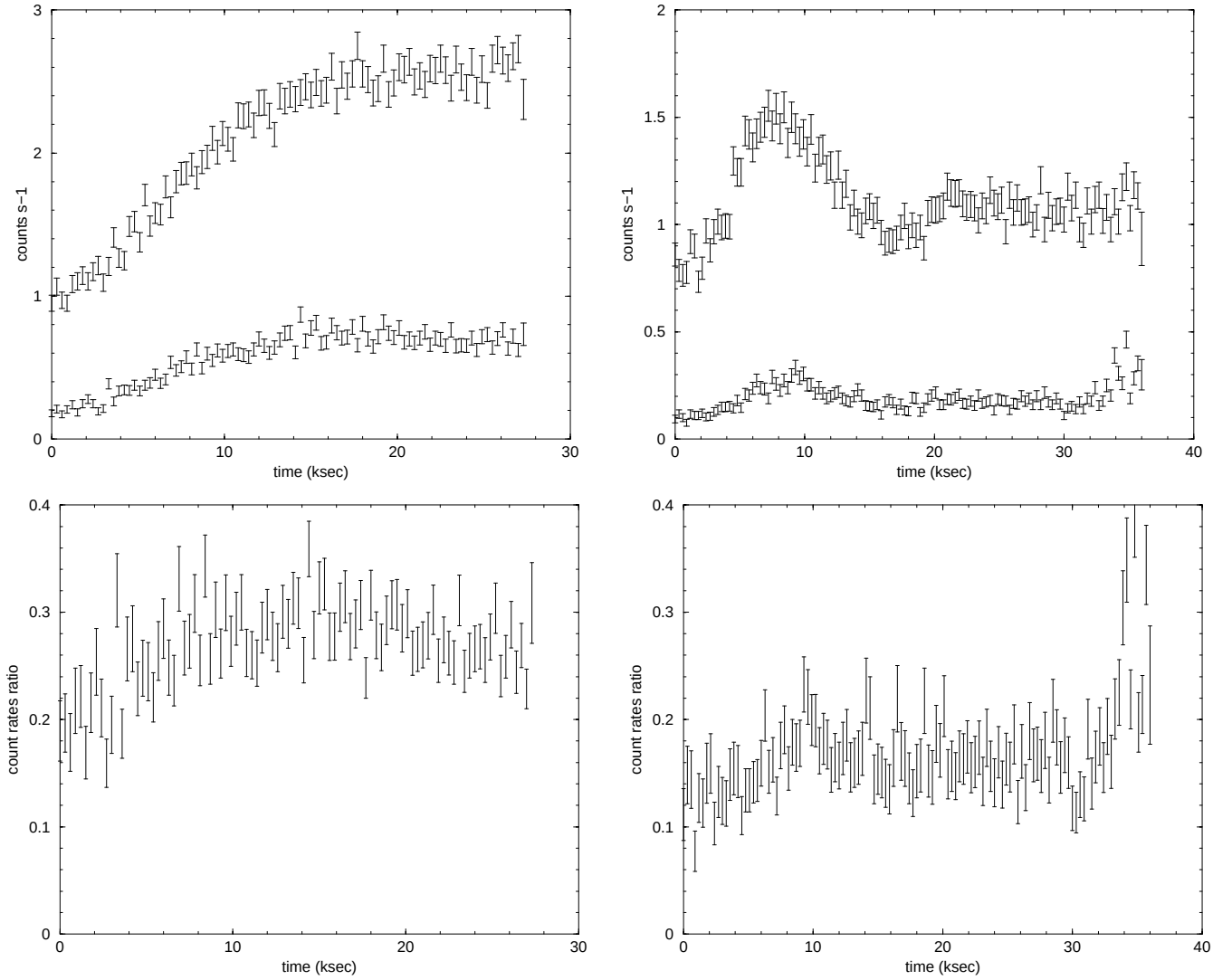

Fig. 2. Top: light curves of FK Comae during revolutions 199 (left) and 205 (right) obtained with the EPIC p−n camera. In each graph, the upper curve is the count rate within the 0.5 to 2 keV band and the lower curve is the count rate within the 2 to 10 keV band. Bottom: 2–10 keV over 0.5–2 keV count rate ratio during revolutions 199 (left) and 205 (right). The events are binned in 300 s time intervals.

The X-ray spectrum of FK Comae was harder during revolution 199 (see Fig. 2 bottom). The X-ray luminosity was higher in the 2−10 keV band than in the 0.3−2 keV band. In spite of a large increase in X-ray luminosity, hr did not change much during revolution 199. The relative increase of the X-ray flux was similar in the low and high energy band suggesting a geometrical origin of the count rate variation. One possible explanation is the progressive emergence of bright X-ray material at the limb of the star. Since the duration of the flux increase was approximately 20 ksec compared with the 2.4 days stellar rotation period, the extent of this bright X-ray region would be about 30 degrees in longitude. According to this hypothesis, this region would have entered the visible hemisphere of FK Comae at the beginning of revolution 199 and would have been fully visible during the last 10 ksec of this revolution. During revolution 205, on the contrary, the X-ray luminosity remained higher in the soft 0.3−2 keV band than in the 2−10 keV band even during the transient high count rate event corresponding to what is hereafter referred as a flare.

5. Spectral analysis of EPIC data

5.1. The 0.3 to 10 keV energy band

We separately fitted the four EPIC datasets (see Fig. 3) with the MEKAL optically thin plasma emission model (Mewe et al. 1985). The interstellar hydrogen column density was fixed to $N_{\rm H} = 1.3 \times 10^{20}$ cm^{-2}, a low value since FK Comae is located near the North Galactic Pole. Using Bohlin et al. (1978) ratio of reddening to hydrogen column density, this $N_{\rm H}$ value gives a V band extinction $A_V = 0.07$ consistent with Burstein & Heiles (1982) reddening estimate assuming an A_V extinction to reddening ratio of 3.2. No single temperature plasma model that

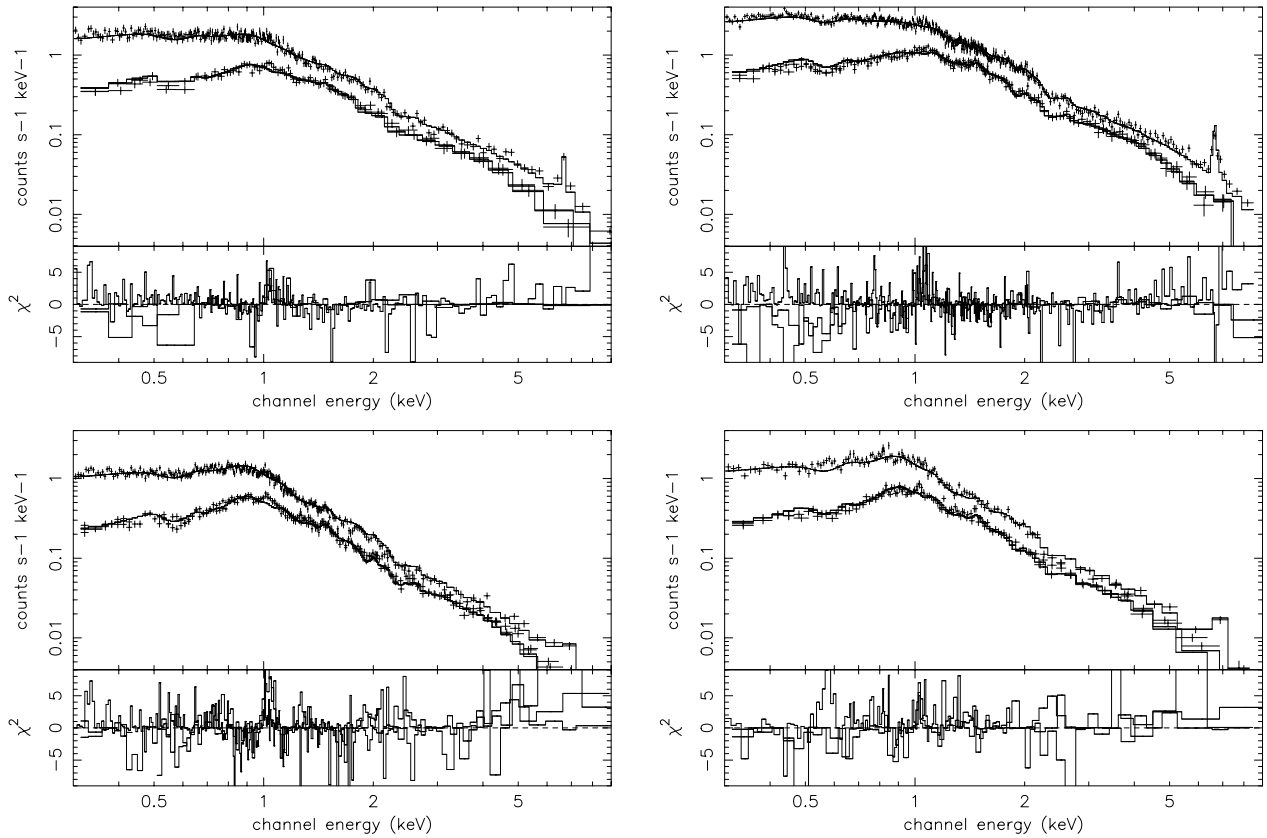

Fig. 3. Top: best fit model to Rev. 199 spectra during the rising flux period (left) and during the high steady flux period (right). Bottom: best fit model to Rev. 205 spectra during the low steady flux period (left) and during the short flare period (right). The EPIC data (crosses) and spectral fit (solid line) are shown in the upper panel and the χ^2 contributions in the lower panel of each graph.

Table 4. Best fit parameters to EPIC data using a 2 component MEKAL model (Mewe et al. 1985) and an hydrogen column density of 1.3×10^{-20} cm^{-2}.

Obs.	Abundance	Low T	Component	High T	Component	
	Z	kT (keV)	EM (10^{52} cm^{-3})	kT (keV)	EM (10^{52} cm^{-3})	χ^2
Rev. 199 (rising cr)	0.36 ± 0.04	0.76 ± 0.02	37 ± 8	5.3 ± 0.2	343 ± 5	0.80
Rev. 199 (high cr)	0.52 ± 0.03	0.74 ± 0.02	23 ± 3	4.8 ± 0.1	585 ± 5	1.04
Rev. 205 (low cr)	0.39 ± 0.02	0.71 ± 0.07	41 ± 4	3.3 ± 0.1	182 ± 3	1.41
Rev. 205 (flare)	0.66 ± 0.04	0.71 ± 0.09	34 ± 4	3.7 ± 0.1	218 ± 5	1.19

assumes either solar photospheric (Anders & Grevesse 1989) or non solar abundances can fit the data, as unacceptably large values of χ^2 were obtained. The MEKAL plasma models with two components at different temperatures prove adequate for all dataset (see Table 4). No improvement to the fit was obtained by adding a third temperature component.

The temperature of the cool plasma component is relatively constant (≈0.7 keV) for all datasets. Hot ($T >$ 3 keV) plasma on FK Comae is the main source of X-ray emission both in the soft and in the hard X-ray band. It contributes to more than 70% of the soft X-ray luminosity in the 0.3−2 keV range and to more than 98% of the luminosity above 2 keV (see Table 3). Table 4 shows that

FK Comae's X-ray luminosity variations both in the soft (<2 keV) and in the hard (>2 keV) range are almost entirely related to change in the emission measure of the hot ($T > 3$ keV) plasma whose temperature was higher during revolution 199 ($T \approx 5$ keV) when the X-ray luminosity was higher.

Assuming identical abundances in the two plasma components, the average element abundance in FK Comae corona is found to be lower than the solar photospheric value (see Table 4). The derived abundances are significantly higher during the high count rate periods of both revolution 199 and 205 data ($Z = 0.6 \pm 0.1$) than during the respective low count rate periods ($Z = 0.37 \pm 0.05$). This behavior is reminiscent of metallicity enhancements which have been reported during stellar flares, e.g. on Algol (Ottman & Schmitt 1996; Favata & Schmitt 1999), on the RSCVn like binary II Peg (Mewe et al. 1997), on the weak-lined T Tauri star V773 Tau (Tsuboi et al. 1998), and on the dMe star EV Lac (Favata et al. 2000).

5.2. The Fe K line

One major feature of FK Comae spectrum is the presence of a high energy tail and of an emission feature around 6.7 keV attributed to an iron K emission line (see Fig. 4). A second component also appeared at 6.94 keV during revolution 199 when the X-ray emission flux of FK Comae was maximum. The iron Kα fluorescence line consists of two components Kα_1 and Kα_2 at 6.404 keV and 6.391 keV respectively for Fe I and a branching ratio of 2:1 (Bambynek et al. 1972). The natural width of the lines ($\Delta E \approx 3.5$ eV) and any broadening due to thermal motions of the emitting atoms ($\Delta E(\mathrm{eV}) \approx 0.4(T/10^6)^{1/2}$) are negligible compared to the energy resolution (155 eV *FWHM*) of the EPIC cameras. The iron Kα fluorescent line energy is an increasing function of the ionization state. It rises slowly from 6.40 keV in Fe I to 6.45 keV in Fe XVII (neon-like) and then increases steeply with the escalating number of vacancies in the L-shell to 6.7 keV in Fe XXV and 6.9 keV in Fe XXVI (House 1969; Makishima 1986). Spectral fits to the EPIC p−n spectra above 3 keV by a powerlaw and a Gaussian line model give energy positions of the Fe K line equal to $6.67^{+0.04}_{-0.05}$ keV for all datasets (see Table 5). This result indicates that iron was in a high Fe XXV state of ionization during all observations. The second line component at 6.94 keV during revolution 199 suggests a small contribution from Fe XXVI ions during maximum flux levels. For a collisionally dominated optically thin coronal plasma, the Fe XXV ion concentration reaches a maximum value in the $2\text{–}7 \times 10^7$ K temperature range (Raymond-Smith 1977), in agreement with the temperature of the hot plasma component derived by spectral fitting. The increase of the Fe K line peak intensity during the high count rate periods of revolution 199 and 205 also indicates that the line is emitted by the hot plasma component. This confirms the thermal origin of the Fe K emission.

Table 5. Phenomenological model of the Fe K line. Best fit parameters to EPIC p−n data using a power law and a Gaussian line model in the 3 to 10 keV spectral range.

Obs.	Γ	Energy (keV)	σ (eV)	*EW* (eV)
Rev. 199 (rising cr)	2.00 ± 0.07	6.69 ± 0.02	33 ± 64	411
Rev. 199 (high cr)	2.04 ± 0.05	6.65 ± 0.01	51 ± 25	431
Rev. 205 (low cr)	2.42 ± 0.11	6.65 ± 0.03	56 ± 66	390
Rev. 205 (flare)	2.35 ± 0.17	6.68 ± 0.03	54 ± 68	723

Among all of the different changes, eruption and instabilities which are seen on the Sun, the ones which are labelled "flares" all have in common material heated to temperatures of 10^7 K or higher (Golub & Pasachoff 1997). Such temperatures are not seen in the non-flaring corona, and events which do not produce such hot plasma do not seem to be called flares. Thus, by analogy with the Sun, the existence of significant amounts of 10^7 K material in the corona of FK Comae and the detection of Fe XXV emission may be taken as basic flare indicators. The increase of the hot plasma emission measure and of its associated Fe XXV emission both during the short transient event of revolution 205 and during the steady flux increase in revolution 199 indicate that these two events are related to flaring activity. This is consistent with the view that the short transient event during revolution 205 is due to a single flare. On the other hand, the steady flux increase during revolution 199 would result from the gradual emergence of a large volume of hot plasma at the limb of the star corresponding to several flares occurring within the same region. This region could have been overlaying a giant photospheric spot similar to those mapped using Doppler imaging techniques (Strassmeier et al. 1999). The observations performed during revolutions 199 and 205 are separated by 12.3 days, i.e. 5.1 rotation periods of FK Comae. Hence, the same hemisphere of the star was visible during the two observations. The emission measure of the hot plasma which was measured during revolution 199 was about two times smaller 12.3 days later. However, the observation of a transient event at this time is consistent with the hypothesis that the hot emitting plasma observed during revolution 199 is associated with flares in a longlived localized region.

6. Spectral analysis of RGS data

6.1. Line identification and fluxes

Because of the lower effective area and larger spectral resolution of the RGS experiment compared with the

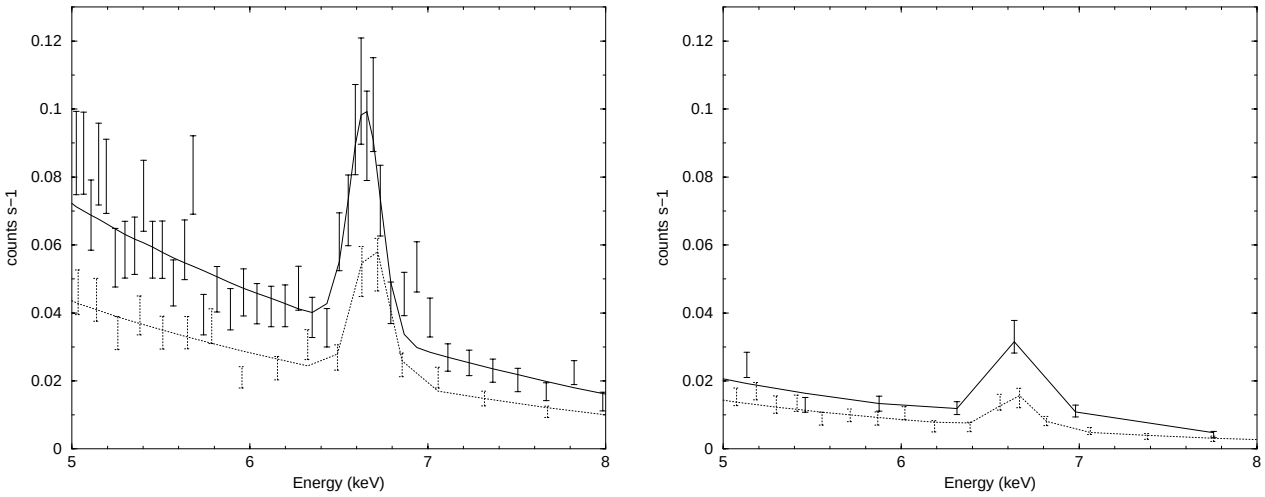

Fig. 4. Left: profile of the Fe K line measured in revolution 199 during the rising flux period (dotted line) and during the high steady flux period (solid line). Right: profile of the Fe K line measured in revolution 205 during the low steady flux period (dotted line) and during the short flare period (solid line). The solid and dotted lines line represent the best fit to the data (error bars) in the 3 to 10 keV region by a phenomenological model consisting of a power law and a Gaussian profile. The same scale was used in both graphics to ease comparison.

EPIC camera, we did not divide the RGS exposures in periods corresponding to low and high count rates. Instead, we compared the RGS spectrum averaged over revolution 199 with the one averaged over revolution 205. This approach provides higher signal to noise ratio spectra at the expense of time resolution. EPIC analysis results shall be kept in mind which indicate that, during revolution 199, the FK Comae corona was dominated by a large emerging region associated with several flares. Aside from a single flare, the star's corona was in average quieter during revolution 205.

Figure 5 shows the RGS spectra averaged over revolution 199 and over revolution 205. Each spectrum is the sum of the two spectra simultaneously obtained with the RGS1 and RGS2 reflection grating spectrometers on board *XMM-Newton*. For line identification, we required only that the wavelength coincidence be comparable to the spectral resolution of the RGS spectrometers, namely 0.04 Å over the 5 to 35 Å wavelength range. In the X-ray domain, many candidate lines may exist within this acceptable wavelength coincidence range. Hence, we only looked for resonance transitions of abundant elements and predicted line intensities using spectra of the Sun (Doschek & Cowan 1984) and of Capella (Brinkman et al. 2000). Serie of lines of highly ionized Fe and several lines of the Ly and He series are visible in RGS spectra, most notably from C, N, O and Ne. The strongest lines are listed in Table 6. Their temperatures of maximum formation range between 2 and 10 MK indicating that the corresponding ions are associated with the cool plasma component inferred from EPIC data.

When comparing the spectra obtained during revolution 199 and 205, the most obvious difference is the higher continuum emission observed at short wavelengths during revolution 199. This continuum is mainly associated with the bremstrahlung emission from the high temperature ($T > 10^7$ K) plasma derived from EPIC data which most contributes to the overall X-ray luminosity of FK Comae during revolution 199. Line fluxes were measured using the "migrad" minimization method of XSPEC by fitting the RGS spectra with Gaussian profiles, which represent the observed line profiles very well. The continuum emission of the hot plasma component was modelized by a bremstrahlung component at a temperature of 3.5 keV (rev. 205) and 5.1 keV (rev. 199) as derived from spectral fitting of EPIC data. The bremstrahlung model was normalised on the overall RGS spectral range. Line fluxes corrected for interstellar absorption on the line of sight to FK Comae ($N_{\rm H} = 1.3 \times 10^{20}$ cm^{-2}) are given in Table 6. Flux measurements of the Si XIII (6.7 Å), Ne X (12.13 Å), O VIII (16.01 Å) and Fe XVII (17.05 Å) lines are affected by blends. No significant difference of line intensities are seen between revolutions 199 and 205 thus confirming that FK Comae X-ray variability between the two revolutions is due to emission measure variations of hot plasma most likely associated with flares. The presence of a variable bremstrahlung component and of a stable emission line component in RGS spectra supports the use of a two temperature plasma model for the interpretation of the EPIC data. Although this model is a simplified approximation, it indicates that the emission measure distribution of the plasma in the corona of FK Comae exhibit two peaks at distinct temperatures.

6.2. Fitting of the emission line spectrum

Since the cool plasma component is responsible for the line emission spectrum of RGS and is relatively stable in temperature during revolution 199 and 205, we simultaneously fitted the low energy RGS spectra obtained in revolution 199 and 205 by a single temperature VMEKAL model with variable abundances. The model generates

Table 6. Measured positions and fluxes of the strongest lines in the RGS spectra of FK Comae obtained during revolutions 199 and 205. The columns give the predicted line positions, the measured line positions during revolution 199, the measured line positions during revolution 205, the ion and line identifications, the temperatures of maximum line formation, the line fluxes measured during revolution 199 and the line fluxes measured during revolution 205.

$\lambda_{\rm pred}$ (Å)	$\lambda_{\rm rev199}$ (Å)	$\lambda_{\rm rev205}$ (Å)	Ion	line ID	$\log(T_{\rm m})$ log (K)	$F_{\rm rev199}$ ($10^{-6}\,{\rm cm^{-2}\,s^{-1}}$)	$F_{\rm rev205}$ ($10^{-6}\,{\rm cm^{-2}\,s^{-1}}$)
6.65	6.70		Si XIII	He4w	7.00	30 ± 27	
6.74		6.75	Si XIII	He6z	7.00		6 ± 120
12.13	12.13	12.17	Ne X	H1AB	6.80	42 ± 13	70 ± 15
12.12			Fe XVII	4C	6.75		
13.45	13.43	13.46	Ne IX	He4w	6.60	33 ± 12	28 ± 9
15.01	15.01	15.02	Fe XVII	3C	6.70	18 ± 7	32 ± 7
16.01	16.00	16.00	O VIII	H2	6.60	14 ± 4	14 ± 5
16.07			Fe XVIII	F3	6.80		
16.79	16.78	16.79	Fe XVII	3F	6.70	6 ± 5	9 ± 4
17.05	17.06	17.06	Fe XVII	3G	6.70	37 ± 11	27 ± 9
17.10			Fe XVII	M2	6.70		
18.97	18.96	18.96	O VIII	H1AB	6.50	42 ± 8	41 ± 7
21.61	21.60	21.57	O VII	He4w(r)	6.50	22 ± 6	7 ± 5
21.80	21.81		O VII	He5xy(i)	6.30	4 ± 5	<5
22.12	22.10	22.11	O VII	He6z(f)	6.30	6 ± 5	4 ± 5
24.78	24.78	24.76	N VII	H1AB	6.30	10 ± 8	8 ± 8
33.74	33.70	33.64	C VI	H1AB	6.10	9 ± 10	7 ± 0.2

a spectrum of hot diffuse gas with line emission from several elements based on the calculation of Mewe et al. (1985) with Fe L calculations by Liedahl (1995). A single electron temperature and electron density is assumed for the entire ensemble of element charge states and in particular for iron, oxygen and neon which produce the most prominent lines. This highly simplified assumption turns out to be fairly adequate within the observational uncertainties of the present spectrum. The fit was performed in the spectral range from 10 Å to 20 Å where the efficiency of the RGS spectrometers is the highest. An initial abundance of 0.45 was used, as established by the MEKAL model. The temperature and abundances of the Fe, O and Ne elements which give prominent lines in the considered spectral range were then allowed to vary. The fitting results are given in Table 7. They corroborate the EPIC data analysis and indicate that the emission measure distribution of the plasma in FK Comae exhibits a peak around 0.7 keV. This is reminiscent of the emission measure distribution found from the EUV observations of Capella (G1 III + G8 III) (Dupree et al. 1993; Schrijver et al. 1995; Brickhouse et al. 2000). It is worth noting that *Chandra* observations (Behar et al. 2001) have also shown that the iron-L spectrum of Capella between 10 Å and 18 Å can be reproduced almost entirely by assuming a single electron temperature of $kT = 0.6$ keV. The single temperature simplication is apparently a reasonable modeling assumption for the soft X-ray emission line spectra of active giants. The average abundance derived from the RGS spectra of FK Comae is consistent with the analysis results of EPIC data. However, the Ne abundance is significantly higher than the average value and the Fe and O abundances are slightly lower. Hence, the Ne/O ratio found for FK Comae is unusually high compared with the solar photospheric value. This Ne enhancement is reminiscent of a similar anomaly observed in a subset of solar flares (Murphy et al. 1991; Schmelz 1993).

Table 7. Best fit parameters to RGS spectra recorded in revolution 199 and 205 using a VMEKAL model with variable Fe, O and Ne abundance.

Parameter	Value
kT (keV)	0.76 ± 0.01
Fe	0.27 ± 0.01
O	0.33 ± 0.03
Ne	1.18 ± 0.14
Other abundances	0.45
χ^2	1.16 (1669/1693 d.o.f.)

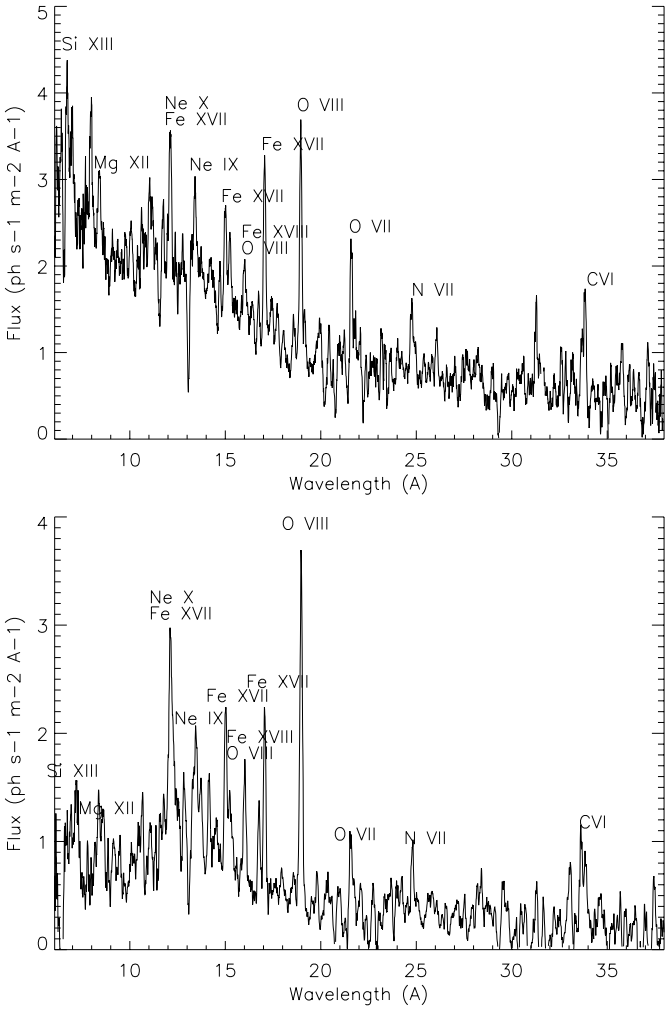

Fig. 5. Averaged first order spectra of RGS 1 and 2 obtained during revolutions 199 (top) and 205 (bottom).

6.3. The helium-like O VII triplet

Information on the emitting volume of the different plasma components could be derived if their electron densities were known. Electron densities can be measured using density sensitive spectral lines originating from metastable levels, such as the forbidden (f) 2^3S-1^1S line in helium like ions. This line and the associated resonance (r) 2^1P-1^1S and intercombination (i) 2^3P-1^1S lines make up the so-called helium like triplet lines (Gabriel & Jordan 1969; Pradhan 1982; Mewe et al. 1985). The intensity ratio $(i+f)/r$ varies with electron temperature and the ratio i/f varies with electron density due to the collisional coupling between the metastable 2^3S upper level of the forbidden line and the 2^3P upper level of the intercombination line.

The RGS wavelength band contains the He-like triplets from O VII, Ne IX, Mg XI and Si XIII. However, the Si and Mg triplets are not sufficiently resolved and the Ne IX triplet is too heavily blended with iron and nickel lines for unambiguous density analysis. Only the O VII lines are clean, resolved and potentially suited to diagnose plasmas in the density range $n_e \approx 10^8-10^{11}$ cm^{-3} and temperature range $T \approx 1$–9 MK. However, the temperature of the cool plasma component ($T \approx 0.75$ keV i.e. 8.7 MK) is significantly larger than the temperature ($T = 2$ MK) of maximum abundance of the O VII ions, hence the low line intensities of the O VII triplet. This effect combined with the absence of RGS 2 data in this spectral range prevents an accurate measurement of the intercombination to forbidden line ratio. A rough estimate of the i/f ratio is 1.5 for revolution 199, which implies (Pradhan 1982) a density $n_e \approx 6 \times 10^{10}$ cm^{-3} for a temperature of 0.75 keV. Unfortunately, the uncertainty on the i/f ratio only allows to ascertain a lower limit $n_e > 2 \times 10^9$ cm^{-3} of the electron density during revolution 199. No estimate could be performed from the revolution 205 data due to the even lower flux.

7. Discussion

7.1. Structure of FK Comae corona

Huenemoerder et al. (1993) predicted that X-ray flux and hardness would vary with rotation in FK Comae. Their idea was that a corotating circumstellar structure, perhaps similar to a quiescent solar prominence, as inferred from Balmer line observations, will partially absorb the X-rays producing a weaker and apparently harder spectrum as it passes in front of the visible hemisphere. We observed flux and hardness changes (see Table 3) but they increased together, contrary to Huenmoerder et al. (1993) prediction, in agreement with Welty & Ramsey (1994) observations. If corotating structures are responsible for the X-ray variability observed, our spectral analysis indicate that they are strong sources of X-rays. We interpreted the steady flux increase during revolution 199 as the gradual emergence of several flares at the limb of the star occurring within a same region. This region is remarkable both by its extent estimated to 30 degree in longitude and by the large emission measure of the associated hot 5−6 keV plasma. Such a high temperature plasma and the iron K−shell blend at 6.7 keV constitute flare indicators which have been detected from the Sun and from non-solar coronae (van den Oord & Mewe 1989; Tsuru et al. 1989). We interpreted the transient event observed during revolution 205 as a single flare. Assuming that the emission measure increase of the hot (>3 keV) plasma during revolution 205 is due to a single flare, the visible hemisphere of FK Comae could have been covered by more than 10 simultaneous giant flares at the end of revolution 199. Intense flaring activity on FK Comae is supported by an average metallicity enhancement during high count rate periods and by a Ne abundance enhancement relative to oxygen reminiscent of abundance anomalies observed during stellar and solar flares. The good fit to FK Comae spectra obtained with a two component model suggests a corona configuration with little contribution from quiet regions similar to the Sun. On the contrary the 0.7 keV temperature of the "cool" component is reminiscent of solar type active regions, while the hot ($T > 3$ keV) may be caused by

disruptions of magnetic fields associated to a permanent flaring activity.

The review of coronal activity by Vaiana & Rosner (1978) pointed out that the Sun, if completely covered with active regions, would have an X-ray luminosity of 2×10^{29} ergs s^{-1}. When scaled to FK Comae surface, an X-ray luminosity of 7 to 20×10^{30} erg s^{-1} is obtained. This value is lower than the observed FK Comae luminosity (30 to 100×10^{30} erg s^{-1}) but higher than the X-ray luminosity contribution (3.7 to 6.3×10^{30} erg s^{-1}) of its cool ($T < 1$ keV) plasma component. Following a simple rule of thumb, an FK Comae surface with a 30 to 50% surface filling factor of bright solar like active regions could probably explain the X-ray luminosity of its "cool" ($T < 1$ keV) plasma component. Assuming that this component is produced by a simple static loop system consisting of N similar loops of constant pressure p (dyn cm^{-2}), temperature T(K) = 0.73 keV, and cross section A (cm^2), the emission measure EM (cm^{-3}) can be expressed as:

$$EM = GF(4\pi R^2)(p/2kT)^2 L \quad (1)$$

where R is the stellar radius, F is the filling factor and L the loop half-length. G is a geometry factor which includes effect of partial occultation of the corona by the star itself (i.e. G varies from 0.5 to 1 for $L \ll R$ to $L \gg R$). Using the relation $T = 1400(pL)^{1/3}$ (Rosner et al. 1978) and $G = 0.7$, a characteristic loop length scale is obtained (Mewe et al. 1982):

$$L_{10} = 7.4 F T_7^4 EM_{52}^{-1} (R/R_\odot)^2 \quad (2)$$

where L_{10} is the loop half length in units of 10^{10} cm, T_7 is the coronal temperature in unit of 10^7 K, and EM_{52} is the emission measure in units of 10^{52} cm^{-3}. Inserting the observed temperature and emission measure of the low count rate period of revolution 205 (see Table 4) and $R = 7.9\ R_\odot$ (see Table 1), we find $L \approx 6$ F $\times 10^{10}$ cm^{-3}. Assuming a 50% filling factor, we derive the corresponding value of loop base pressure and half-length (see Table 8). Since it turns out that the loop length are much smaller than the pressure scale height H, the assumption of constant pressure in the loops is justified. Also it is worth noting that the corresponding electron density is consistent with the lower limit $n_e > 2 \times 10^9$ cm^{-3} derived from the RGS spectra of the O VII helium-like triplet. Characteristic FK Comae loop size and temperature are respectively 3×10^{10} cm and 8.5×10^6 K. For comparison, solar corona observations show bright hot loops within active regions which reach maximum temperatures and electron densities above the neutral line of typically $3{-}4 \times 10^6$ K and 10^{10} cm^{-3} (Vaiana et al. 1973). In addition to these hot loops, on-disk images of the Sun show that neighboring active regions are often connected into complexes of activity by large loop-like structures (Van Speybroek et al. 1970). These interconnecting loops can be $>10^{10}$ cm long, i.e. as long as the loop length estimate on FK Comae. However, they tend to be cooler than loops within solar active regions and therefore cooler than coronal loops on FK Comae.

Table 8. Physical parameters of FK Comae coronal loops.

T (K)	EM (cm^{-3})	H (cm)	L (cm)	n (cm^{-3})
8.5×10^6	41×10^{52}	125×10^{10}	3×10^{10}	6×10^9

With the straightforward deduction that in FK Comae, the cool plasma component is produced by solar like active regions covering 30 to 50% of the star's surface, it is easy to imagine that such a dense population of active regions coexists with constant interaction and disruption of their magnetic fields which might be expected to lead to continuous flaring. This could explain the permanent emission measure of hot plasma at 3 to 5 keV. Different approaches have been proposed to estimate characteristic parameters and in particular the size of flaring regions. Analytic approaches (van den Oord & Mewe 1989; Pallavicini et al. 1990; Hawley et al. 1995) using only rise and decay time are adequate for the analysis of large flare for which only light curves are available. However, they tend to overestimate the size of the flaring regions, in particular in the presence of significant heating during the decay (Favata & Schmitt 1999). As an extreme example, assuming that the short transient event during revolution 205 is related to a single flare event, we estimated the maximum size of this flare by equating the measured decay time, the so-called e-folding time, to the radiative cooling time (Pallavicini et al. 1990), i.e. $\tau_{\rm rad} = 3kT/nP(T)$ where n is the density, T the coronal temperature, k the Boltzmann constant and $P(T)$ the radiative loss function for unit emission measure. $P(T) \approx 2 \times 10^{-23}$ erg cm^3 s^{-1} for temperatures in the range $1 \times 10^7 - 4 \times 10^7$ K (Mewe et al. 1985). We then derived an upper limit to the flare emitting volume V from the measured emission measure $EM = n^2\ V.EM$ was estimated from the emission measure difference of high temperature plasma (see Table 4) between the flare period and the low flux period of revolution 205. By further assuming a single loop model with an aspect ratio $\alpha = 0.1$, we found an upper limit to the loop length of about 2×10^{11} cm (see Table 9), i.e. significantly smaller than FK Comae diameter ($\approx$8 to 14×10^{11} cm).

Covino et al. (2001) showed that the volumes and densities of stellar flares provided by the Pallavicini et al. (1990) approach are not too dissimilar from those derived from the hydro-dynamic decay-sustained heating model of Reale et al. (1997). These authors showed by simulation and verified with *Yokhoh* observations of solar flares that flare decay approximately along a straight line in the $\log EM^{1/2} - \log T$ diagram. They found a relation $f(\chi) = \tau_{\rm lc}/\tau_{\rm th}$ between the slope χ of the decay path and the ratio between the observed decay time $\tau_{\rm lc}$ and the thermodynamic cooling time of the loop without additional heating $\tau_{\rm th}$. The loop length L is proportional to the characteristic decay time, but in the presence of

Table 9. Physical parameters of FK Comae flare during revolution 205 compared with solar compact and two-ribbon flares (Moore et al. 1980; Wu et al. 1986).

	Solar compact flare	Solar 2-ribbon flare	FK Comae flare
$L_{\rm X}$ (erg s^{-1})	10^{26}–10^{27}	10^{27}–10^{28}	10^{31}
τ (s)	10^{2}–10^{3}	10^{4}	1.7×10^{4}
T (K)	$(1-3) \times 10^{7}$	$(1-3) \times 10^{7}$	4×10^{7}
EM (cm^{-3})	10^{48}–10^{49}	10^{49}–10^{50}	36×10^{52}
n (cm^{-3})	10^{11}–10^{12}	10^{10}–10^{11}	$>5.3 \times 10^{10}$
V (cm^{3})	10^{26}–10^{27}	10^{28}–10^{29}	$<10^{32}$
L (cm)	$(0.5-5) \times 10^{9}$	10^{10}	$<2 \times 10^{11}$
$B_{\rm min}$ (G)	100–300	50–100	>100

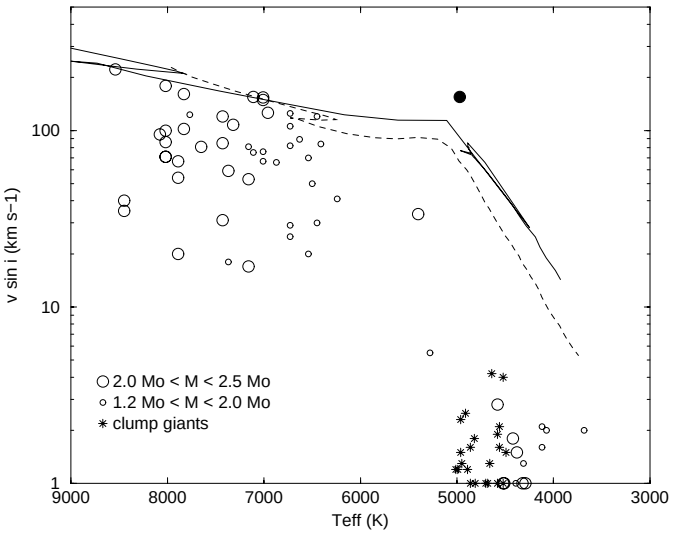

Fig. 6. Rotational velocities of FK Comae (filled circle) with respect to single field giants (Gondoin 1999). The dotted line and the solid line describe the equatorial velocity evolution of 1.7 $M_{\odot}$ and 2.5 $M_{\odot}$ stars respectively assuming angular momentum conservation and $v \sin i = 150$ km s^{-1} at $T_{\rm eff} = 7000$ K.

significant heating during the decay, L is significantly reduced by a factor $f(\chi) > 1$, i.e. (Reale 2001):

$$L_9 = \tau_{\rm lc}.T_7^{1/2}/120.f(\chi) \quad (3)$$

where L_9 and T_7 are in units of 10^9 cm and 10^7 K. When applied to the single flare event observed during revolution 205 (i.e. $\tau_{\rm lc} = 1.7 \times 10^4$ s and $T = 4 \times 10^7$ K), a loop length $L = 2.8 \times 10^{11}/f(\chi)$ cm is obtained. Without high enough count rates for time resolved spectroscopy during rev. 205 flare, the slope χ of the locus of point in the $\log EM^{1/2} - \log T$ diagram cannot be estimated. Therefore, the correction factor $f(\chi)$ is unknown. In a large fraction of the solar flares examined by Reale et al. (1997) significant heating is present, so that the thermodynamic decay time of the loop alone overestimates its size by factors between 2 and 10. A factor $f(\chi)$ of 2 to 4 was found by Favata et al. (2000) in a systematic analysis of four large flares observed on the eclipsing binary Algol with *GINGA*, *EXOSAT*, *ROSAT* and *BeppoSAX*. Assuming similar long lasting heating during the decay phase of rev. 205 flare, loop length in the range 3–14 $\times 10^{10}$ cm are obtained which are greater than the characteristic size (see Table 8) of the static loops derived from the emission measure of the cool plasma component. The X-ray flare on FK Comae would be comparable in size to the two-ribbon flares observed on the Sun (see Table 9). Such evolving loop arcades are the result of different physical processes than the single, constant-volume loop which are assumed in Reale et al. (1997) analysis. They are an alternative possibility to the compact flare scenario that we assumed. This would imply different physical conditions compared to the hydrodynamic simulation of Reale et al. (1997), and thus even larger uncertainties on the interpretation of the transient event observed during revolution 205.

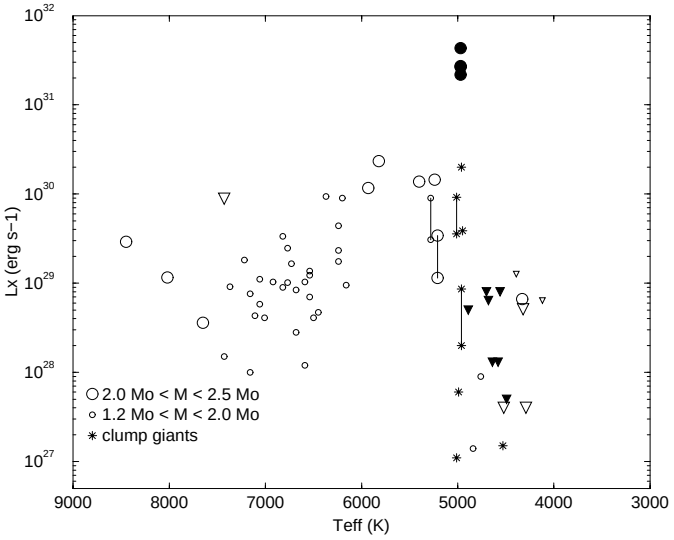

Fig. 7. *XMM-Newton* luminosities of FK Comae (filled circles) in the 0.3 to 2 keV band compared with ROSAT PSPC measurements of single field giants (Hünsch et al. 1998). Upper limits of X-ray luminosities measured with the Einstein observatory (Maggio et al. 1990) are indicated by small triangles, large triangles and filled triangles for low-mass (1.2 $M_{\odot} < M <$ 2.0 $M_{\odot}$), intermediate-mass (2.0 $M_{\odot} < M <$ 2.5 $M_{\odot}$) and clump giants respectively.

7.2. Evolution of FK Comae corona

Possible hypotheses regarding FK Comae origin (see Sect. 2) include evolution from either a single progenitor or from the merging of a close binary system. Although difficult to probe, this second scenario could be expected to produce abundance anomalies in the atmosphere of

the merger, which would last as it becomes a cool giant. Our X-ray measurements show that the average element abundance in FK Comae corona is about half the solar photospheric value. No abundance anomaly is found outside the abundance increase with X-ray luminosity and the Ne abundance enhancement that can be attributed to flares. The single progenitor hypothesis remains a likely scenario providing that it accounts for the rapid rotation of the star. Recent values for FK Comae $v \sin i$ are 159 ± 4 km s^{-1} (Rucinski 1990), 162.5 ± 3.5 km s^{-1} (Huenemoerder et al. 1993) and 155 ± 3 km s^{-1} (Korhonen et al. 1999). The star's photometric period is 2.4002466 ± 0.0000056 days (Jetsu et al. 1993).

In Sect. 2, we calculated the radius of FK Comae from its luminosity and effective temperature and we used the well determined rotational period to estimate its unprojected equatorial velocity. A comparison with the $v \sin i$ value indicates that FK Comae is observed perpendicularly to its rotational axis. This effect together with the large radius of the star's envelope already explains part of its high projected rotational velocity.

We compared the projected rotational velocity of FK Comae with $v \sin i$ values of A-F giants extracted from the Bright Star Catalogue and with $v \sin i$ measurements of G-K giants obtained with CORAVEL by de Medeiros & Major (1995). The CORAVEL measurements are precise to about 1 km s^{-1}. All projected equatorial velocity measurements are plotted in Fig. 6 as a function of $T_{\rm eff}$ for different mass ranges. A-F giants ($T_{\rm eff} > 6000$ K) have high rotational velocities, often greater than 100 km s^{-1}. K giants, on the contrary, have low $v \sin i$ values of 1 or 2 km s^{-1} for $T_{\rm eff} < 4700$ K. As noticed by Simon & Drake (1989), stellar rotation strongly decline during the rapid evolution of G giants across the Hertzsprung gap. Simon & Drake (1989) suggested together with Gray (1989) that magneto-hydrodynamic braking due to stellar winds could explain this phenomenon. Rutten & Pylyser (1988) argued that during the entire evolution of a 3 $M_\odot$ star the timescale for magnetic braking is larger than the evolutionary time scale. Endal & Sofia (1979) and Gray & Endal (1982) pointed out that the expansion of the stars on the red giant branch together with the rearrangement of angular momentum due to the increasing depth of the convection zones may well explain the decrease of $v \sin i$ for cool giants. We calculated the equatorial velocity evolution of 1.7 $M_\odot$ and 2.5 $M_\odot$ giants using Schaller et al. (1992) evolutionary models and assuming angular momentum conservation and $v \sin i = 150$ km s^{-1} at $T_{\rm eff} = 7000$ K. Comparisons with $v \sin i$ measurements (see Fig. 6) confirm that angular momentum conservation alone cannot explain the rotational velocities of K giants. However, Fig. 6 suggests that FK Comae, which is located near the bottom of the RGB, could be evolving just before rotational braking. Angular momentum would have been approximately conserved within its convective envelope during its rapid evolution from mid-F spectral type. A single progenitor hypothesis could then explain the rapid rotation of FK Comae.

Within this hypothesis, the outer convection zone of FK Comae would have deepened since its formation at mid-F spectral type, thus increasing the convective turnover time scale (Gilliland 1985). Since FK Comae only experienced a small spin-down (see Fig. 6) and maintained a high rotation rate, the Rossby number (Durney & Latour 1978) decreased and dynamo activity increased as the star evolved towards the bottom of the RGB. During this period, the deepening convective envelope likely suffered shear stresses, which could have resulted in radial velocity gradients, especially at the interface between the convection zone and the radiative core below it. The necessary conditions were then present to switch on an $\alpha-\Omega$ dynamo with an increasing efficiency as the star evolved towards the bottom of the RGB. Our spectral analysis of the X-ray data suggests that the large fluid kinetic helicity induced by the rapid rotation currently generates magnetic fields with characteristic scale of 3×10^{10} cm, i.e. comparable with large interconnecting solar loops but much smaller than FK Comae diameter. The strong dynamo productive of large magnetic flux induces a large density of active regions covering up to 30−50% of the star surface. We argue that the X-ray emission is strongly enhanced not only due to the occurrence of these large scale magnetic structures, but mainly due to their permanent interactions. These interactions lead to an uninterrupted flaring activity that generates large volume of hot plasmas.

Since FK Comae could be soon ascending the RGB, we anticipate that its rotation will spin-down dramatically with the effect of increasing its Rossby number and decreasing its helicity related dynamo driven activity. Not only the rotational braking *per se* but also the restoration of rigid rotation could prevent the maintenance of large magnetic structures at the bottom of the red giant branch (Gondoin 1999). Rosner et al. (1995) pointed out that this suppression of a large scale dynamo leads to the disappearance of large scale organized stellar magnetic fields but does not imply the suppression of magnetic field production at small scale, driven by the turbulent motion in the surface convection zones. A bifurcation in magnetic loop sizes could occur as the dynamo induced by rotation gives way to a turbulent field generation mechanism like that described by Durney et al. (1993). According to this scenario, X-ray emission from active regions and large flares should progressively disappear as FK Comae evolve from G to K spectral type (see Fig. 7).

The above evolution scenario implies that, from the successive effects of convection zone deepening and rotational braking, a minimum value of the Rossby number is expected around FK Comae evolutionary stage. At this stage, $\alpha - \Omega$ dynamo mechanisms should operate with a maximum efficiency. Since hot coronal plasma conforms the geometry of the magnetic field, the X-ray luminosity of FK Comae shall be within the highest among single giants. We compared our X-ray flux measurements of FK Comae (see Sect. 4) in the 0.3 to 2 keV band with X-ray fluxes of single field giants extracted from

the ROSAT all-sky survey catalogue (Hünsch et al. 1998). Upper limits of *Einstein* X-ray fluxes were also retrieved from Maggio et al. (1990). We calculated the X-ray luminosities ($L_{\rm X}$) of all stars from the Hipparcos parallaxes. The results are presented in Fig. 7 as a function of $T_{\rm eff}$ for different mass ranges. The X-ray emission of giants reaches a maximum value in the effective temperature range 6000 K $< T_{\rm eff} <$ 5000 K corresponding to G spectral types. Figure 7 confirms that the X-ray luminosity of FK Comae is the highest within this sample of single nearby F, G and K giants, thus supporting the above evolution scenario.

8. Summary

Our analysis of FK Comae data suggests that the corona of FK Comae is dominated by the same type of active region structure as on the Sun. However, the surface area coverage of these active regions approaches 50% and the size of the associated magnetic structures can be similar or larger than that of interconnecting loops between solar active regions while their temperature is hotter. The interaction of these structures themselves most likely explains the permanent flaring activity on large scales that is responsible for heating FK Comae plasma to coronal temperatures of $T \geq 10^7$ K. These flares are not randomly distributed on the star surface. During our observations, they were partly grouped within a large compact region of about 30 degree extent in longitude. We speculate that this coronal region with a large density of flares could have been overlaying a giant photospheric spot. Based on FK Comae position in the H-R diagram, we anticipate that FK Comae rotation will spin-down in the future with the effect of decreasing its helicity related, dynamo driven activity and suppressing large scale magnetic structures in its corona.

Acknowledgements. We thank our colleagues from the *XMM-Newton* Science Operation Center for their support in implementing the observations. We are grateful to D. F. Favata and to the anonymous referee for providing helpful comments on the manuscript.

References

Anders, E., & Grevesse, N. 1989, Geochim. Cosmochim. Acta, 53, 197
Arnaud, K., & Dorman, B. 2001, XSPEC User's Guide for version 11.1, `http://heasarc.gsfc.nasa.gov/docs/xanadu/xspec/manual/manual.html`
Bambynek, W., Craseman, B., Fink, R. W., et al. 1972, Rev. Mod. Phys., 44, 716
Behar, E., Cottam, J., & Kahn, S. M. 2001, ApJ, 548, 966
Bohlin, et al. 1978, ApJ, 224, 132
Bopp, B. W., & Rucinski, S. M. 1981, in IAU Symp. 93, Fundamental Problems in the Theory of Stellar Evolution, ed. D. Sugimoto et al. (Dordrecht: Reidel), 177
Bopp, B. W., & Stencel, R. E. 1981, ApJ, 247, L231
Brickhouse, N. S., Dupree, A. K., Edgar, R. J., et al. 2000, ApJ, 530, 387
Brinkman, A. C., Gunsing, C. J. T., Kaastra, J. S., et al. 2000, ApJ, 530, 111
Burstein, D., & Heiles, C. 1982, AJ, 87, 1165
Collier Cameron, A. 1982, MNRAS, 200, 89
Covino, S., Panzera, M. R., Tagliaferri, G., et al. 2001, A&A, 371, 973
den Herder, J. W., Brinkman, A. C., Kahn, S. M., et al. 2001, A&A, 365, L7
de Medeiros, J. R., & Mayor, M. 1995, A&A, 302, 745
Doschek, G. A., & Cowan, R. D. 1984, ApJS, 56, 67
Dupree, A. K., Brickhouse, N. S., Doschek, G. A., et al. 1993, ApJ, 418, 41
Durney, B. R., & Latour, J. 1978, Geophys. Astrophys. Fluid Dyn., 9, 241
Durney, B. R., De Young, D. S., & Roxburgh, I. W. 1993, Sol. Phys., 145, 207
Eggen, O. J., & Iben, I. J. 1989, AJ, 97, 431
Ehle, M., Breitfellner, M., Dahlem, M., et al. 2001, The *XMM-Newton* Users' Handbook, `http://xmm.vilspa.esa.es/user/AO2/uhb/xmm_uhb.html`
Endal, A. S., & Sofia, S. 1979, ApJ, 232, 531
ESA 1997, The Hipparcos Catalogue, ESA SP-1200
Favata, F., & Schmitt, J. H. M. M. 1999, A&A, 350, 900
Favata, F., Reale, F., Micela, G., et al. 2000, A&A, 353, 987
Flower, P. J. 1996, ApJ, 469, 335
Gabriel, A. H., & Jordan, C. 1969, MNRAS, 145, 241
Gilliland, R. L. 1985, ApJ, 299, 286
Golub, L., & Pasachoff, J. M. 1997, in The Solar Corona (Cambridge University Press, Cambridge UK)
Gondoin, P. 1999, A&A, 352, 217
Gondoin, P., Aschenbach, B., Erd, C., et al. 2000, SPIE Proc., 4140, 1
Gray, D. F. 1989, ApJ, 347, 1021
Gray, D. F., & Endal, A. S. 1982, ApJ, 254, 162
Hawley, S. L., Fisher, G. H., Simon, T., et al. 1995, ApJ, 453, 464
Holtzman, J. A., & Nations, H. L. 1984, AJ, 89, 391
House, L. L. 1969, ApJS, 18, 2
Huenemoerder, D. P., Ramsey, L. W., Buzasi, D. L., et al. 1993, ApJ, 404, 316
Hünsch, M., Schmitt, J. H. M. M., & Voges, W. 1998, A&AS, 127, 251
Hughes, V. A., & McLean, B. J. 1987, ApJ, 313, 263
Jansen, F., Lumb, D., Altieri, B., et al. 2001, A&A, 365, L1
Jetsu, L., Pelt, J., & Tuominen, I. 1993, A&A, 278, 449
Korhonen, H., Berdyugina, S. V., Hackman, T., et al. 1999, A&A, 346, 101
Liedahl, D. A., Osterheld, A. L., & Goldstein, W. H. 1995, ApJ, 438, 115
Maggio, A., Vaiana, G. S., Haisch, B. M., et al. 1990, ApJ, 348, 253
Makishima, K. 1986, in The Physics of Accretion onto Compact Objects, ed. K. O. Mason, M. G. Watson, & N. E. White (Springer Verlag, Berlin), 250
McCarthy, J. K., & Ramsey, L. W. 1984, ApJ, 283, 200
Mewe, R., Gronenschild, E. H. B. M., Heise, J., et al. 1982, ApJ, 260, 233
Mewe, R., Gronenschild, E. H. B., & van den Oord, G. H. J. 1985, A&A, 62, 197
Mewe, R., Kaastra, J. S., van den Oord, G. H. J., et al. 1997, A&A, 320, 147

Murphy, R. J., Ramaty, R., Reames, D. V., et al. 1991, ApJ, 371, 793
Oliveira, J. M., & Foing, B. H. 1999, A&A, 343, 2130
Ottmann, R., & Schmitt, J. H. M. M. 1996, A&A, 307, 813
Pallavicini, R., Tagliaferri, G., & Stella, L. 1990, A&A, 228, 403
Pradhan, A. K. 1982, ApJ, 263, 477
Raymond, J. C., & Smith, B. W. 1977, ApJS, 35, 419
Reale, F., Betta, R., Peres, G., et al. 1997, A&A, 325, 782
Reale, F. 2001, in Stellar Coronae in the Chandra and XMM Era, ASP Conf. Ser., TBD, 2001, ed. F. Favata, & J. Drake
Rosner, R., Tucker, W. H., & Vaiana, G. S. 1978, ApJ, 220, 643
Rosner, R., Musielak, Z. E., Cattaneo, F., et al. 1995, ApJ, L442, L25
Rucinski, S. M. 1990, PASP, 102, 306
Rutten, R. G. M., & Pylyser, E. 1988, A&A, 191, 227
SAS 2001, *XMM-Newton* Science Analysis System, Reference Documentation, `http://xmm.vilspa.esa.es/user/sas_top.html`
Schaller, G., Schaerer, D., Meynet, G., & Maeder, A. 1992, A&AS, 96, 269
Schmelz, J. T. 1993, ApJ, 408, 373
Schrijver, C. J., Mewe, R., van den Oord, G. H. J., & Kaastra, J. S. 1995, A&A, 296, 477
Simon, T., & Drake, S. A. 1989, ApJ 346, 303
Strassmeier, K. G., Bartus, J., Cutispoto, G., et al. 1997, A&AS, 125, 11
Strassmeier, K. G., Lupinek, S., Dempsey, R. C., et al. 1999, A&A, 347, 212
Strüder, L., Briel, U., Dennerl, K., et al. 2001, A&A, 365, L18
Trimble, V., & Kundu, A. 1997, AJ, 115, 358
Tsuboi, Y., Koyama, K., Murakami, H., et al. 1998, ApJ, 503, 894
Tsuru, T., Makishima, K., Ohashi, T., et al. 1989, PASJ, 41, 679
Turner, M. J. L. T., Abbey, A., Arnaud, M., et al. 2001, A&A, 365, L27
Vaiana, G. S., Davis, J. M., Giacconi, R., et al. 1973, ApJ, 185, 47
Vaiana, G. S., & Rosner, R. 1978, ARA&A, 16, 393
van den Oordt, G. H. J, & Mewe, R. 1989, A&A, 213, 245
Van Speybroeck, L. P., Krieger, A. S., & Vaiana, G. S. 1970, Nature, 227, 818
Walter, F. M. 1981, ApJ, 245, 677
Walter, F. M., & Basri, G. S. 1982, ApJ, 260, 735
Welty, A. D., & Ramsey, L. W. 1994, AJ, 108, 299